Stratigraphy and taphonomy of tubular macrofossils in Terreneuvian rocks of the Soltanieh Formation, Soltanieh Mountains, Northern Iran

Najmeh Etemad-Saeed [a, b, *], Ross P. Anderson [c, d], Nicholas J. Tosca [e], Kristin D. Bergmann [b], Andrew H. Knoll [f]

[a] Institute for Advanced Studies in Basic Sciences (IASBS), Department of Earth Sciences, Zanjan 45137-66731, Iran

[b] Massachusetts Institute of Technology, Department of Earth, Atmospheric and Planetary Sciences, Cambridge, MA 02139, USA

[c] University of Oxford, Department of Earth Sciences, Oxford, OX1 3AN, UK

[d] University of Oxford, All Souls College, Oxford OX1 4AL, UK

[e] University of Cambridge, Department of Earth Sciences, Downing Street, Cambridge, CB2 3EQ, UK

[f] Harvard University, Department of Organismic and Evolutionary Biology, Cambridge, Massachusetts 02138, USA

*Corresponding author email: n.etemad@iasbs.ac.ir; najmeh83@mit.edu

ABSTRACT

Unmineralized tubular remains with variable morphology and preservability are common in Ediacaran and Cambrian rocks, providing important records of early animal evolution. Here we report a new occurrence of such fossils in the Soltanieh Mountains of northwestern Iran. A large, densely packed tube population is present in the lowermost part of low-energy, outer shelf mudrocks of the Fortunian Upper Shale Member (USM) of the Soltanieh Formation in the Jashn Sara section. Morphologically, these tubes are unbranched and straight to sinuously curved, with uniform diameters of 0.8-1.1 mm and lengths up to 34 mm. The fossils are preserved as orangish to cream-colored structures with low positive relief. X-ray diffraction and SEM-EDS reveal that Soltanieh tubes were largely infilled by variable mixes of pyrite framboids (and their oxidation products), silica, and clay minerals. In contrast, the sediment matrix is dominated by K-Al-silicate with lesser amounts of an Al-oxide/(oxy)hydroxide phase. The abundance of pyrite in the tubes indicates a prominent role for sulfate-reducing bacteria in the post-mortem decay of organic materials within the tubes, and abundant chert along the tube's inner margins further indicates the propensity of silica to precipitate on relatively recalcitrant organic structures. While the newly discovered population shares features in common with *Sabellidites cambriensis*, known from Terreneuvian strata in northern Europe and Avalonia, the Iranian fossils do not preserve the transverse annulations characteristic of *Sabellidites* walls. With this in mind, we leave our new population in open nomenclature. Nonetheless, the occurrence of abundant organic-walled tubes in the USM of the Soltanieh Formation adds to both the diversity of animal fossils found regionally in Terreneuvian rocks and the broader paleogeographic distribution of tubular metazoans in early Cambrian oceans.

Keywords: Tubular macrofossils, Fortunian; Upper Shale Member; Soltanieh Formation; Soltanieh Mountains; Gondwana

1. Introduction

Fossils document the tempo, mode, and environmental context of animal evolution in Cambrian oceans. Mineralized skeletons (Maloof et al., 2010), unmineralized organic remains (Briggs, 2015), and trace fossils (Mángano and Buatois, 2020) record distinct aspects of Cambrian diversification, requiring that paleontologists draw on all three to build an integrated account of early animal evolution. This, in turn, necessitates the analysis of stratigraphic relationships in successions that preserve multiple types of records, along with chemostratigraphic data, especially carbon and strontium isotopes, that facilitate correlation (e.g., Bowyer et al., 2022; Maloof et al., 2010; Wood et al., 2019). Although straightforward in principle, the task is complicated by both the distinct environmental preferences of different taxa and taphonomic circumstances.

Here we focus on the thick, mixed carbonate-siliciclastic succession of the Soltanieh Formation, exposed in the Soltanieh Mountains of northwestern Iran. Small shelly fossils (SSFs; Hamdi et al., 1989; Devaere et al., 2021), trace fossils (Shahkarami et al., 2017a, 2017b; Famarini Bozchamouei et al., 2020), and isotopic chemostratigraphy (Etemad-Saeed et al., 2021) have previously been described from sections within this basin. To this increasing record, we add the occurrence of unmineralized tubular macrofossils, broadly similar to macroscopic tubes found widely in lower Cambrian rocks.

2. Geological setting

The Soltanieh Mountains of northern Iran contain a thick and well-preserved succession of Ediacaran-Cambrian sedimentary rocks, deposited along the western margin of Gondwana (papers cited in Etemad-Saeed et al., 2021). The lower part of the succession, dominated by siliciclcastic rocks, is up to 1100 m thick; the contact with underlying bedrock is not exposed (e.g., Honarmand et al., 2016; Etemad-Saeed et al., 2021). Designated as the Kahar Formation, this lower package is generally ascribed to the late Ediacaran Period, an interpretation supported by ca. 550 Ma detrital zircons mid-succession (Honarmand et al., 2016). Kahar rocks are conformably overlain by a ca. 1000 m mixed siliciclastic-carbonate succession, the Soltanieh Formation. This formation, which is the focus of this study, contains unambiguous early Cambrian body and trace fossils, but as discussed further below, the precise placement of the Ediacaran-Cambrian boundary within the formation remains a topic of debate.

Previous interpretations of Kahar and Soltanieh paleoenvironments suggest a fluvial to siliciclastic tidal environment that changes upward into peritidal carbonates interbedded with deeper water siliciclastic-dominated shelf deposits (Etemad-Saeed et al., 2021; Shahkarami et al., 2017a).

Northeast of Jashn Sara village, 23 km southwest of the city of Zanjan in northwestern Iran (36° 36′ 9.60″ N, 48° 14′ 47.87″ E; Fig. 1A), the Kahar and Soltanieh formations are exposed in the Jashn Sara Section. Here, the Kahar Formation consists mainly of ~400 m of green to grey mudrock and sandstone, with subordinate intercalations of dark gray stromatolitic dolomite (Fig. 1B). Kahar strata are conformably overlain by ca. 1100 m of mixed carbonate-siliciclastic strata assigned to the Soltanieh Formation (Fig. 1B). At Jashn Sara, Soltanieh strata are conformably overlain by the upper Terreneuvian (Stage 2) Barut Formation, characterized by the regular alteration of purple/red mudrocks and grey stromatolitic dolomite. The contact is gradational and placed arbitrarily at the base of the first colored (mainly purple) shale intercalation (Stöcklin et al., 1965).

At Jashn Sara, the Soltanieh Formation consists of five members: the Lower Dolomite Member (LDM), Lower Shale Member (LSM), Middle Dolomite Member (MDM), Upper Shale Member (USM), and Upper Dolomite Member (UDM), ranging in age from latest Ediacaran to Cambrian Stage 2, based on SSFs, trace fossil evidence and regional chemostratigraphy (Etemad-Saeed et al., 2021; Famarini Bozchalouei et al., 2020; Hamdi et al., 1989). The LDM comprises ~70 m of dark stromatolite-bearing dolomites, whereas the overlying LSM contains ~198 m of greenish-gray, paper-to-platy shale, representing a regional highstand. In turn, the ~75 m thick MDM consists predominantly of gray to brown, well-bedded to massive dolomites. The USM, which hosts the tubular fossils described in this study in its lowermost part, comprises an approximately 77 m succession of grey to light-yellowish papery to fissile shales without evidence of cross beds or ripples, again representing relatively quiet off-shore environments deposited at a highstand (Figs. 1B, 2A–C). These basinal mudrocks shallow upward to alternating shales/sandstones/phosphatic dolomites towards the top of the USM. Finally, the overlying UDM contains ~690 m of buff-colored to brown, medium-bedded to massive stromatolitic dolomite, interbedded with mixed greenish-gray mudrock and thinly stratified, fine-grained sandstone (Figs. 1B, 2D).

2.1 Age of Soltanieh Formation

Hamdi et al. (1989) first reported SSFs from the Soltanieh Formation, placing the base of the Cambrian within the LSM based on the first appearances of *Hyolithellus* sp., *Rugatotheca* sp., *Protohertzina* sp., and an unnamed fossil interpreted as a monoplacophoran. More diverse Fortunian fossils, including *Anabarites trisulcatus*, *Cambrotubulus decurvatus*, and *Protohertzina anabarica*, occur within the MDM and basal USM (see also Ciabeghodsi, 2007). In more recent research, Devaere et al. (2021), corroborated the conclusions of Hamdi et al. (1989) and further proposed that the transition from the Fortunian to Cambrian Stage 2 is most probably located in the lower part of the USM as described in the Central Alborz locality, based on the highest occurrence of Fortunian taxa, including *Maikhanella multa* and *Purella squamulose*.

In contrast, trace fossil assemblages have been used to place the base of the Cambrian at the base or within the LDM (Shahkarami et al., 2017a, 2017b) due to the first appearances o*f Helminthoidichnites tenuis, Helminthopsis tenuis*, and *Cochlichnus anguineus,* interpreted as a distal expression of the *Treptichnus pedum* zone in light of the SSF data noted above. They also placed the base of Cambrian Stage 2 in the UDM, noting a marked change in the abundance and complexity of trace fossils. Famarini Bozchalouei et al. (2020), however, maintain that the Ediacaran-Cambrian boundary is higher in the Jashn Sara section, placing it about 8 m above the base of the MDM, based on the first appearance of *Treptichnus pedum per se*.

Carbon isotopes support the placement of the base of the Cambrian in the LDM, as these beds show the pronounced negative $\delta^{13}C$ anomaly observed globally in basal Cambrian rocks (Etemad-Saeed et al., 2021). Differences in the placement of the Ediacaran–Cambrian boundary within the Soltanieh Formation may be explained by the varied environmental preferences of the organisms represented by the diverse skeletal and trace fossils used as evidence. Devaere et al. (2021), in particular, cautioned that stratigraphic occurrences of skeletal and trace fossils can vary markedly based on environmental preferences (Landing et al., 2013; see also Wilson et al., 2012). In any event, all paleontological and chemostratigraphic interpretations place the tubular fossils reported in this study within the Fortunian Stage of the Cambrian Period.

3. Materials and methods

130 fossiliferous mudrock samples were collected from the lowermost 18 m of the USM in the Jashn Sara Section (Fig. 2A). All samples contain conspicuous tubular fossils, which seem to be distributed more or less evenly through this interval.

Samples were cleaned with distilled water and an air-blower and photographed under a Zeiss SteREO binocular microscope at different magnifications, at the Department of Earth, Atmospheric and Planetary Sciences, MIT. The length, width (in the middle and at both ends), and orientation of each tube were measured from the photographs using ImageJ and GEOrient, and various aspects of their morphology were documented, including the shape of terminations, branching, folding, evidence of structure in the walls, and whether tubes overlapped. The left and right ends were determined arbitrarily only for comparing differences in size between the ends of an individual specimen. Table S1 and Figures S1-S7 provide a detailed description of the sample population.

To investigate tube and matrix composition, thin sections taken from 40 different individuals were prepared and studied using a polarizing Zeiss Axio Imager M2 microscope, at the Department of Earth, Atmospheric and Planetary Sciences, MIT (Fig. S8).

To determine the mineralogical composition of the tubes, selected-area *in situ* X-ray diffraction (XRD) was performed using a PANalytical Empyrean diffractometer, with a Co Kα source and PIXcel-1D detector, at the Department of Earth Sciences, University of Oxford. This *in situ* technique limits the irradiated area to 7x1 mm, across the entire two-theta range of the scan using programmable divergence slits, enabling individual tubes to be analyzed, though the thickness of the sample from which diffraction arises likely extends more than 50-100 μm in depth (for detailed methods and a comparison between in situ XRD and more commonly used powder XRD, see Anderson et al., 2021). XRD was undertaken on 10 fossil tubes from four hand samples (for locations see Fig. S9). In addition, XRD of matrix material from three of the four hand samples (n=3 analyses per sample) was performed for comparison. Relative mineral abundances were calculated using the reference intensity ratio method (Snyder and Bish, 1989) with Highscore software (https://www.malvernpanalytical.com/en/products/category/software/x-ray-diffraction-software/highscore).

Scanning electron microscopy (SEM) was performed on a subset of the polished slabs to investigate the textural relationships between the fossils and associated minerals. Slabs were carbon coated and analyzed using a FEI Quanta 650 Emission Gun SEM at the Department of

Earth Sciences, University of Cambridge, operated at an accelerating voltage of 15 kV under high vacuum with a dwell time of 10 μs. The SEM is also equipped with an energy dispersive X-ray detector to facilitate semi-quantitative chemical analysis via energy dispersive X-ray spectroscopy (EDS) using the AZtec software suite (Oxford Instruments). EDS analyses were conducted with a 50 mm detector, aperture of 3, and spot size of 4 using an approximate 2nA beam current.

4. Results

4.1. Tube Morphology

Relatively dense, monospecific assemblages of tubular fossils are preserved as compressions with low positive relief (Fig. 3A, 3B). The tubes are mostly straight to sinuously curved, although rare individuals form nearly complete circles (Fig. 4A–D). In life, these organisms must have had strong but somewhat flexible walls. Tube length ranges between 4.6 and 34 mm, with a mean size of 14.8 mm (stdev=6.47, n=127), but insofar as most individuals are incomplete, they were presumably longer (Table S1; Fig. 5). Tube width ranges from 0.3 to 2.2 mm (mean=0.8, stdev=0.32, n=127) at the left end, 0.4 to 2.7 mm (mean=1.1, stdev=0.34, n=127) in the middle, and 0.3–1.8 mm (mean=0.8, stdev=0.32, n=127) at the right end, indicating a uniform thickness along the length of the tubes. The difference between the widths of each end in individual tubes ranges between 0 and 1.6 mm (mean=0, stdev=0.33, n=127).

Tube ends can be rounded or squared off, and a few individuals appear to narrow toward one end (Fig. 4A, 4C). Very likely, this variation reflects the orientation of tubes relative to the bedding plane. The sample population shows no evidence of branching, and overlap of compressed tubes is rare. In some hand samples tubes show a distinct darker wall-like structure that is distinct from tube infilling (Fig. 6A–C), and rare individuals show possible evidence of fine transverse annulations (Fig. 6D). In general, however, the tubes are preserved by post-mortem infilling, leaving us uncertain about surface textures of the original walls. Measurement of tube orientations shows that while populations on individual bedding planes can show some alignment, preferred orientations vary markedly from one bed to the next, likely reflecting post-mortem alignment by currents, feeding behavior, or both (Table S1; Figures S1-S7).

4.2. Tube Composition

Tubes have striking dark to pale orange, brown, or cream colors that stand in marked contrast to their surrounding matrix (Fig. 3A, 3B), prompting the question of their composition.

SEM-EDS data reveal that all fossil specimens are composed, almost exclusively, of variable mixes of pyrite (now mostly transformed to Fe-oxides) and silica (Figs. 7A–B, 8A–B). The morphology of individual pyrite crystals is well preserved, with most occurrences being octahedral/cuboidal forms no larger than approximately 1 μm in size, but commonly smaller than this. The pyrite crystals are largely clustered into well-defined framboids on the order of 15 μm in diameter, and numerous pyrite framboids are dispersed within tubular fossils and aggregated around their exteriors (Figs. 7C–D and 8C–D). Some specimens show clear evidence for oxidation of pyrite to Fe-oxides, which likely imparts their orange color. In these specimens, framboidal structures yield high Fe and low-S compositions (not shown) in EDS and exhibit a change in morphology from the octahedral/cuboidal crystals typical of pyrite to fibrous or other poorly defined morphologies. In addition to pyrite framboids and Fe-oxides, fossil interiors are enriched in silica relative to the sediment matrix (Figs. 7D, 8D).

In contrast, the SEM-EDS data indicate that the sediment matrix is dominated by a K-Al-silicate with lesser amounts of an Al-oxide/(oxy)hydroxide phase (i.e., gibbsite, diaspore, or boehmite). The latter phase is sometimes concentrated at the edges of some fossils, and in one case, appears to constitute a significant proportion of the fossil interior (Fig. 9). The sediment matrix also contains pyrite but less commonly as framboids. Compared to the fossils, pyrite within the sediment matrix is more evenly distributed and occurs in smaller total amounts.

XRD analysis (n=19) indicates that both tubes (n=10) and their surrounding matrix (n=9) yield diffraction peaks consistent with a kaolin-group mineral (i.e., kaolinite or dickite; 0–7%), illite (20–57%), muscovite (15–44%), and quartz (26–52%) (Fig. 10). Kaolinite and muscovite are slightly elevated in the matrix (mean: Kaolinite = 1%, muscovite = 28%) compared to the tubes (mean: Kaolinite = 0%, muscovite = 23%), whereas illite and quartz are slightly elevated in the tubes (mean: illite = 40%, quartz = 37%) compared to the matrix (mean: illite = 35%, quartz = 35%). The interquartile ranges, however, overlap in comparisons between the matrix and tubes for all minerals suggesting differences in mean values should not be given significance.

When compared to SEM data, *in situ* XRD data help assign mineral species to major components of the samples. There are, however, notable differences between the two techniques. For example, given the mm to cm control on the size and shape of the analytical footprint associated with *in situ* XRD, and accounting for interaction volumes reaching approximately 100 μm depth in the sample, any one analysis likely reflects a mixture of fossil and sediment matrix area. As such, the stark mineralogical and compositional contrasts between the fossils and matrix, clearly apparent in SEM-EDS data (Figs. 7, 8, 9), are only subtly apparent using this technique (Fig. 10). Additionally, *in situ* XRD does not detect pyrite or Fe-oxides, though they are clearly present in SEM-EDS data. This may result from the relatively small crystallite size of both phases, which would broaden associated diffraction peaks and decrease their intensity. Furthermore, the high degree of preferred orientation among layer silicate minerals in most mudrocks means that *in situ* XRD reflects a disproportionately large contribution from layer silicate mineral 001 reflections, increasing their abundance at the expense of other phases.

5. Discussion

5.1. Taphonomy

While the Soltanieh tubes contain clay minerals, they are largely infilled by (originally) pyrite and chert. Pyrite suggests a prominent role for sulfate-reducing bacteria in the post-mortem decay of organic materials within the tubes, with bacterially generated sulfide reacting with ferrous iron in ambient pore waters (Farrell, 2014). The lower abundance of pyrite in adjacent mudstone is consistent with a higher concentration of organic matter in the tubes, relative to their matrix, providing a locus of sulfate reduction. The presence of iron oxides reflects diagenetic pyrite oxidation, as observed, for example, in the late early Cambrian Skyberg Lagerstätte in southern Norway (Høyberget et al., 2023) and "rusty" sabelliditids preserved by oxidized iron infillings from the Digermulen Peninsula, northern Norway (Ebbestad et al., 2022). The high concentration of chert within tubes, and especially adjacent to their margins (accounting for the cream color evident in some specimens), may reflect the propensity of silica to precipitate on cell walls and other organic features (e.g., Knoll, 1985).

In general, then, the current mineralogy of the fossils appears to reflect early diagenetic anaerobic respiration of labile organic materials inside the tubes by sulfate-reducing bacteria (Gabbott et al., 2004), while the wall remained intact, serving as a substrate for silicification within voids developed within the less labile tube walls as internal tissues decayed. Precipitation of an Al-oxide/(oxy)hydroxide phase around tube exteriors reflects later diagenesis, as does an unidentified dark material lining some specimens – perhaps Mn-oxides emplaced during the late diagenetic oxidation that converted much pyrite to iron oxides.

5.2. Taxonomy

Several groups of extant animals live in tubes, and tubular fossils are common in late Ediacaran to basal Cambrian rocks, so much so that Schiffbauer et al. (2016) wrote of a global "worm world" fauna, while Budd and Jackson (2016) christened this interval the "tube world." Unmineralized tubular remains are thought to include animal body fossils as well as trace fossils and algal compressions.

Simple organic tubes preserved with walls intact occur as large populations in carbonaceous shales of the Nama Group, Namibia, dated at 545–539 Ma (Cohen et al., 2009; Nelson et al., 2022). These fossils have been compared to the possibly algal *Vendotaenia* (Gnilovskaya, 1971), but their sediment infilling and consequent three-dimensional morphology suggest that animal affinities should also be considered. The Nama tubes are comparable to the Soltanieh fossils in width, but in general, are more than an order of magnitude longer.

Fossils more securely interpreted as algal occur widely in rocks of the late Ediacaran to Cambrian age, preserved as essentially two-dimensional organic compressions that include tubes. Most, however, can be distinguished from the Soltanieh population on the basis of size, propensity for branching, helical or irregular wall tears, sharp folding, and/or a lack of three-dimensionality (Bykova et al., 2020; e.g., LoDuca et al., 2017; Wang et al., 2022).

Simple tubular trace fossils have also long been described from rocks of this age, although a number of them are now interpreted as body casts and molds (Jensen et al., 2006; Sappenfield et al., 2011). Genuine tubular trace fossils can be distinguished from the Soltanieh population by their size, lack of any evidence for walls, and infilling with sand or other clastic sediment, without penecontemporaneous minerals precipitated biogeochemically.

Perhaps the best known taxon among the organic-walled tubes in basal Cambrian shales is *Sabellidites cambriensis* Yanishevsky (1926). *Sabellidites cambriensis* occurs widely in uppermost Ediacaran and basal Cambrian (Fortunian) shales in northern Europe (Baltica), as well as in the basal Cambrian GSSP in eastern Newfoundland (Avalonia) (Ebbestad et al., 2022). Morphologically, *S. cambriensis* consists of unbranched, mm-scale tubes characterized by distinctive transverse annulations (e.g., Ebbestad et al., 2022). Yanishevky's (1926) original interpretation of *Sabellidites* as an annelid worm was seconded by Sokolov and Iwanowski (1990) and supported by microstructural analyses of preserved walls (Moczydłowska et al., 2014), although some phylogenetic uncertainty persists (e.g., Ebbestad et al., 2022).

In overall size and shape, the Soltanieh population resembles *S. cambriensis*, and it occurs in rocks of comparable age; however, in the absence of well-preserved walls, we cannot confirm whether or not the Iranian fossils share the diagnostic character of transverse annulations. Moreover, *S. cambriensis* specimens tend to be straight or only slightly sinuous, (Ebbestad et al., 2022, and references therein) as opposed to the markedly sinuous to circular morphologies found in Iran, suggesting mechanically distinct wall properties.

Organic-walled tubes from uppermost Ediacaran and lower Cambrian rocks in China expand our sense of both the taxonomic complexity and phylogenetic uncertainty of tubular remains. Yang et al. (2005) described tubular macrofossils from argillaceous limestones of the lower Cambrian

Xidashan Formation in Xinjiang as *S. cambriensis*. In overall size and morphology, this population resembles European *S. cambriensis* populations, but transverse annulations are illustrated in only a single specimen and strong sinuosity is common. Luo and Zhang (1986) erected two additional species of *Sabellidites* from Cambrian rocks of southern China, but these have twice over been reassigned to other genera based on microstructural features not found in *S. cambriensis,* first *Mafangscolex* (Hu, 2005) and more recently *Rugosusivitta* (Tang et al., 2021), interpreted as palaeoscolecids (extinct ecdysozoans) and flatworms, respectively. Moreover, slightly larger tubes with both transverse annulations and longitudinal striations have been described from Terrenuevian rocks of the North China craton, some preserved with iron oxide infillings. Described as *Fuxianospira gyrata* and interpreted as green algae, these tubes are distinguished by helical separations along tube axes (Wang et al., 2022). Dense populations of unattributed tubes also occur in Yunnan (Tang et al., 2021).

As noted above, in the absence of clear evidence for transverse wall annulations, we cannot ascribe the Soltanieh fossils to *S. cambriensis* with any degree of confidence. We cannot rule out that the Iranian fossils are sabelliditids of some sort, but given uncertainties about the nature of any higher taxon to which *S. cambriensis* may have belonged, we choose to leave the Soltanieh population in open nomenclature, while underscoring its similarities to other tube populations distributed widely in rocks of comparable age. Reconstructions of early Cambrian paleogeography commonly situate the West Avalonian microcontinent represented by eastern Newfoundland adjacent, or nearly so, to the Amazonian craton (e.g., Torsvik and Cocks, 2017; Wen et al., 2020), although dissenting views exist (e.g., Landing et al., 2022). The Soltanieh population shows that regardless of where Avalonia is placed, organic-walled tube organisms thrived in marginal seaways of West Gondwana.

6. Conclusions

A large population of tubular fossils found on bedding surfaces of shales in the Upper Shale Member of the Soltanieh Formation, Iran, resembles unmineralized tube-forming animals known previously from uppermost Ediacaran and lower Cambrian (Fortunian) shales in Baltica, West Avalonia, and China. Tube walls are not preserved in the Soltanieh fossils, but first-order features of morphology have been preserved by the diagenetic emplacement of biologically induced pyrite and silica precipitation in tube interiors. Like the skeletal and trace fossils in the Soltanieh Formation, the unmineralized remains reported here suggest strong faunal similarities among mid-latitude shelves and platforms bordering the Iapetus and Prototethys oceans at the beginning of the Cambrian Period.

7. Note on Repository

Fossiliferous slabs are housed in the Department of Earth, Atmospheric and Planetary Sciences, Massachusetts Institute of Technology. Polished slabs are reposited in the Mineralogy Laboratory, University of Cambridge.

Acknowledgments

This work was supported by the Institute for Advanced Studies in Basic Sciences [grant number G2022IASBS52752]; All Souls College (University of Oxford) and the Royal Society [grant numbers: URF\R1\221220, RF\ERE\221057]; and the University of Cambridge and the Leverhulme Centre for Life in the Universe. We thank Katherine Clayton for her help with XRD analyses, Iris Buisman for assistance with SEM-EDS sample preparation and analysis, and S.

Karimi for his assistance during fieldwork. We also thank J.O.R. Ebbestad and an anonymous reviewer for helpful comments that improved this contribution.

References

Anderson, R.P., Tosca, N.J., Saupe, E.E., Wade, J., Briggs, D.E.G., 2021. Early formation and taphonomic significance of kaolinite associated with Burgess Shale fossils. Geology. 49, 355–359.

Bowyer, F.T., Zhuravlev, A.Y., Wood, R., Shields, G.A., Zhou, Y., Curtis, A., Poulton, S.W., Condon, D.J., Yang, C., Zhu, M., 2022. Calibrating the temporal and spatial dynamics of the Ediacaran-Cambrian radiation of animals. Earth. Sci. Rev. 225, 103913.

Briggs, D.E.G., 2015. The Cambrian explosion. Current Biol. 25, R864–R868.

Budd, G.E., Jackson, I.S.C., 2016. Ecological innovations in the Cambrian and the origins of the crown group phyla. Phil. Trans. Royal Soc. B: Biol. Sci. 371, 20150287.

Bykova, N., LoDuca, S.T., Ye, Q., Marusin, V., Grazhdankin, D., Xiao, S., 2020. Seaweeds through time: morphological and ecological analysis of Proterozoic and early Paleozoic benthic macroalgae. Precambrian Res. 350, 105875.

Ciabeghodsi, A., 2007. Biostratigraphy, Chemostratigraphy and Sedimentary environment of Neoproterozoic–Cambrian strata of Alborz Mountains. Ph.D. thesis, Shahid-Beheshti University.

Cohen, P.A., Bradley, A., Knoll, A.H., Grotzinger, J.P., Jensen, S., Abelson, J., Hand, K., Love, G., Metz, J., McLoughlin, N., others, 2009. Tubular compression fossils from the Ediacaran Nama group, Namibia. J. Paleontol. 83, 110–122.

Devaere, L., Korn, D., Ghaderi, A., Struck, U., Bavandpur, A.K., 2021. New and revised small shelly fossil record from the lower Cambrian of northern Iran. Pap. Palaeontol. 7, 2141–2181.

Ebbestad, J.O.R., Hybertsen, F., Högström, A.E.S., Jensen, S., Palacios, T., Taylor, W.L., Agić, H., Høyberget, M., Meinhold, G., 2022a. Distribution and correlation of *Sabellidites cambriensis* (Annelida?) in the basal Cambrian on Baltica. Geol. Mag. 159, 1262–1283.

Etemad-Saeed, N., Knoll, A.H., Najafi, M., Bergmann, K.D., Haseley, N., Karimi, S., 2021a. Carbon isotope chemostratigraphy of a Gondwanan Ediacaran–Cambrian transition, Soltanieh Mountains, northern Iran. Gondwana Res. 99, 163–177.

Famarini Bozchalouei, M., Abbassi, N., Salsani, A., Zohdi, A., 2020. Neoprotrozoic-Cambrian boundary in Soltanieh Formation by the ichnological studies, Seyedkandi section, Soltanieh Mountains, NW Iran. Sci. Quart. J. Geosci. 30, 163–174.

Farrell, Ú.C., 2014. Pyritization of soft tissues in the fossil record: an overview. The Paleontological Society Papers 20, 35–58.

Gabbott, S.E., Xian-Guang, H., Norry, M.J., Siveter, D.J., 2004. Preservation of Early Cambrian animals of the Chengjiang biota. Geology. 32, 901–904.

Gnilovskaya, M.B., 1971. The oldest aquatic plants of the Vendian of the Russian Platform (late Precambrian). Paleont. J. 5, 372–378.

Hamdi, B., Brasier, M.D., Zhiwen, J., 1989. Earliest skeletal fossils from Precambrian-Cambrian boundary strata, Elburz Mountains, Iran. Geol. Mag. 126, 283–289.

Honarmand, M., Li, X.-H., Nabatian, G., Rezaeian, M., Etemad-Saeed, N., 2016. Neoproterozoic-Early Cambrian tectono-magmatic evolution of the Central Iranian terrane, northern margin of

Gondwana: Constraints from detrital zircon U-Pb and Hf-O isotope studies. Gondwana Res. 37, 285–300.

Høyberget, M., Ebbestad, J.O.R., Funke, B., Funke, M.-L.K., Nakrem, H.A., 2023. The Skyberg Lagerstätte from the Mjøsa area, Norway: a rare window into the late early Cambrian biodiversityof Scandinavia. Lethaia 56, 1–28.

Hu, S., 2005. Taphonomy and palaeoecology of the Early Cambrian Chengjiang biota from eastern Yunnan, China. Berlin Palaobiol. Abh. 7, 182–185.

Jensen, S., Droser, M.L., Gehling, J.G., 2006. A critical look at the Ediacaran trace fossil record. In: Neoproterozoic geobiology and paleobiology (S. Xiao, A.J. Kaufman, eds.), Springer Verlag, Dorndrecht, Netherlands, p.115–157.

Jinbiao, C., Huimin, Z., Yusheng, X., Guogan, M., 1981. On the Upper Precambrian (Sinian Suberathem) in China. Precambrian Res. 15, 207–228.

Knoll, A.H., 1985. Exceptional preservation of photosynthetic organisms in silicified carbonates and silicified peats. Phil. Trans. Royal Soc. B, Biol. Sci. 311, 111–122.

Landing, E., Geyer, G., Brasier, M.D., Bowring, S.A., 2013. Cambrian evolutionary radiation: context, correlation, and chronostratigraphy overcoming deficiencies of the first appearance datum (FAD) concept. Earth Sci. Rev. 123, 133–172.

Landing, E., Keppie, J.D., Keppie, D.F., Geyer, G., Westrop, S.R., 2022. Greater Avalonia—latest Ediacaran–Ordovician “peribaltic” terrane bounded by continental margin prisms (“Ganderia,” Harlech Dome, Meguma): Review, tectonic implications, and paleogeography. Earth Sci. Rev. 224, 103863.

LoDuca, S.T., Bykova, N., Wu, M., Xiao, S., Zhao, Y., 2017. Seaweed morphology and ecology during the great animal diversification events of the early Paleozoic: a tale of two floras. Geobiology 15, 588–616.

Luo, H.L., Zhang, S.S., 1986. Early Cambrian vermes and trace fossils from Jinning-Anning region, Yunnan. Acta Palaeontologica Sinica 25, 307–313.

Maloof, A.C., Porter, S.M., Moore, J.L., Dudás, F.Ö., Bowring, S.A., Higgins, J.A., Fike, D.A., Eddy, M.P., 2010. The earliest Cambrian record of animals and ocean geochemical change. Geol. Soc. Am. Bull. 122, 1731–1774.

Mángano, M.G., Buatois, L.A., 2020. The rise and early evolution of animals: where do we stand from a trace-fossil perspective? Interface Focus 10, 20190103.

Moczydłowska, M., Westall, F., Foucher, F., 2014. Microstructure and biogeochemistry of the organically preserved Ediacaran metazoan *Sabellidites*. J. Paleontol. 88, 224–239.

Nelson, L.L., Ramezani, J., Almond, J.E., Darroch, S.A.F., Taylor, W.L., Brenner, D.C., Furey, R.P., Turner, M., Smith, E.F., 2022. Pushing the boundary: a calibrated Ediacaran-Cambrian stratigraphic record from the Nama Group in northwestern Republic of South Africa. Earth Planet. Sci. Lett. 580, 117396.

Sappenfield, A., Droser, M.L., Gehling, J.G., 2011. Problematica, trace fossils, and tubes within the Ediacara Member (South Australia): redefining the Ediacaran trace fossil record one tube at a time. J. Paleontol. 85, 256–265.

Schiffbauer, J.D., Huntley, J.W., O’Neil, G.R., Darroch, S.A.F., Laflamme, M., Cai, Y., 2016. The latest Ediacaran wormworld fauna: setting the ecological stage for the Cambrian explosion. GSA Today, 26, 4–11.

Shahkarami, S., Mángano, M.G., Buatois, L.A., 2017a. Discriminating ecological and evolutionary controls during the Ediacaran–Cambrian transition: trace fossils from the Soltanieh Formation of northern Iran. Palaeogeogr. Palaeoclimatol. Palaeoecol. 476, 15–27.

Shahkarami, S., Mángano, M.G., Buatois, L.A., 2017b. Ichnostratigraphy of the Ediacaran-Cambrian boundary: new insights on lower Cambrian biozonations from the Soltanieh Formation of northern Iran. J. Paleontol. 91, 1178–1198.

Snyder, R.L., Bish, D.L., 1989. Quantitative analysis. Rev. Mineral. Geochem. 20, 101–144.

Sokolov, B.S., Iwanowski, A.B., 1990. The Vendian System, Vol. 1: Paleontology. Springer Verlag, Berlin, 396 p. (English edition)

Stöcklin, J., Nabavi, M., Samimi, M., 1965. Geology and mineral resources of the Soltanieh Mountains (Northwest Iran). Geological Survey of Iran.

Tang, F., Song, S., Zhang, G., Chen, A., Liu, J., 2021. Enigmatic ribbon-like fossil from Early Cambrian of Yunnan, China. China Geol. 4, 205–214.

Torsvik, T.H., Cocks, L.R.M., 2017. Earth history and palaeogeography. Cambridge University Press, 332 p.

Wang P.-L, LoDuca, S.T., Wu, M.-Y., Tang, Y.-G., Sun, Z.-X., 2022. Benthic primary producers in exceptionally preserved Cambrian biotas of North China. Palaeoworld 31, 14-29.

Wen, B., Evans, D.A.D., Anderson, R.P., McCausland, P.J.A, 2020. Late Ediacaran paleogeography of Avalonia and the Cambrian assembly of West Gondwana. Earth and Planetary Science Letters 552, 116591.

Wilson, J.P., Grotzinger, J.P., Fischer, W.W., Hand, K.P., Jensen, S., Knoll, A.H., Abelson, J., Metz, J.M., McLoughlin, N., Cohen, P.A., Tice, M.M., 2012. Deep-water incised valley deposits at the Ediacaran-Cambrian boundary in southern Namibia contain abundant *Treptichnus pedum*. Palaios 27, 252–273.

Wood, R., Liu, A.G., Bowyer, F., Wilby, P.R., Dunn, F.S., Kenchington, C.G., Cuthill, J.F.H., Mitchell, E.G., Penny, A., 2019. Integrated records of environmental change and evolution challenge the Cambrian Explosion. Nat. Ecol. Evol. 3, 528–538.

Yanishevsky, M., 1926. On the remains of the tubular worms from the Cambrian blue clays: Ezhegodnik Russkogo Paleontologicheskogo obshchestva. 4, 99–114.

Yang, R., Zhang, C., Song, G., Liu, X., 2006.Vermicular fossils in the early Cambrian Xidashan Formation in the Quruqtagh region of Xinjiang, China. Progr. Nat. Sci. 16, 559-562.

Figure Captions:

Fig. 1. — Location map and stratigraphy of the study area. **A**) Regional geological map, with the fossil locality marked by a star. **B**) Stratigraphic column for the Jashn Sara section.

Fig. 2. — Field photos from the Jashn Sara section. **A**) Lower part of the Upper Shale Member. Box indicates the approximate position of tubular fossils. **B**) Fissile mudrocks. **C**) Arrow pointing to macroscopic fossils. **D**) Lower part of the Upper Dolomite Member.

Fig. 3. — Abundance and density of tubular fossils preserved as randomly distributed individuals with low positive relief.

Fig. 4. —Tubular macrofossils from the Upper Shale Member of the Jashn Sara section, showing variations in morphology and color: **A**) straight, **B, C**) sinuously curved, and **D**) nearly complete circles.

Fig. 5. — Histograms of tube widths and lengths measured from samples.

Fig. 6. —Tubular macrofossils from the Upper Shale Member of the Jashn Sara section, showing differentiation of wall and infilling materials. **A, B, C**) distinctly darker wall-like structures. **D**) Possible but uncertain evidence of fine transverse annulations.

Fig. 7. — SEM-EDS of fossilized structures from sample 13. **A**) Backscattered electron image of a fossilized structure. Brighter regions correspond to material with higher concentrations of high atomic mass (Z) elements. White box corresponds to analysis region in (C) and (D). **B**) Corresponding EDS map of (A) showing distinct Fe-, Al- and Si-rich regions associated with the structures. **C**) Backscattered electron image of area shown in (A), showing spherical pyrite

framboids, and dispersed finely crystalline pyrite which are variably replaced by Fe-oxides. **D**) Corresponding EDS map of (C).

Fig. 8. — SEM-EDS of fossilized structures from sample 13. **A**) Backscattered electron image of fossilized structure. Brighter regions correspond to material with higher concentrations of high atomic mass (Z) elements. White box corresponds to analysis region in (C) and (D). **B**) Corresponding EDS map of (A) showing that the structure is largely composed of Fe-rich regions (pyrite framboids), embedded in a Si-rich matrix. **C**) Backscattered electron image of area shown in (A), showing spherical pyrite framboids evenly dispersed through the interior of the structure. **D**) Corresponding EDS map of (C).

Fig. 9. — SEM-EDS of fossilized structures from sample 13. **A**) Backscattered electron image of the fossilized structure. Brighter regions correspond to materials with higher concentrations of high atomic mass (Z) elements. **B**) Corresponding Fe map of (A) showing that Fe tends to be concentrated within the interior of the structure. **C**) Corresponding Si map of (A) showing enrichment within the structure relative to the matrix. **D**) Corresponding Al map of (A) showing localized concentration of high-Al material along the edges of the structure. **E**) Corresponding Fe, Si and Al map of (A).

Fig. 10. — XRD data shown as box plots comparing the relative abundance of minerals between *in situ* measurements of fossils (blue) and matrix (orange). X = mean; central line = median; box indicates first and third quartile values; line ends indicate maximum and minimum values.

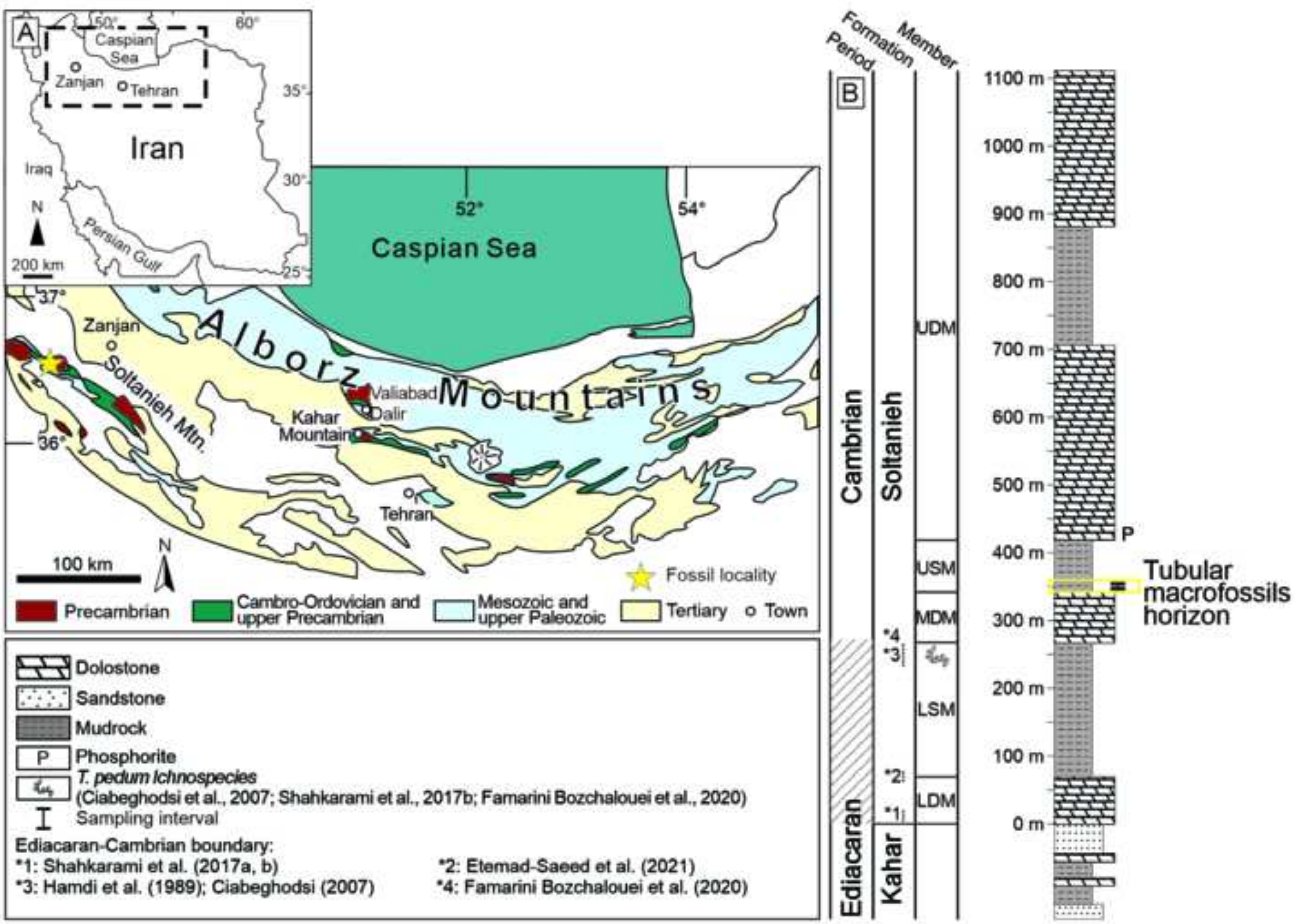
A
50°
60°
Caspian Sea
Zanjan
Tehran
35°
Iran
Iraq
30°
N
Persian Gulf
200 km
25°
52°
54°
Caspian Sea
37°
Zanjan
Alborz Mountains
Soltanieh Mtn.
Valiabad
Dalir
Kahar Mountain
36°
Tehran
100 km
N
Fossil locality
Precambrian
Cambro-Ordovician and upper Precambrian
Mesozoic and upper Paleozoic
Tertiary
Town
Dolostone
Sandstone
Mudrock
Phosphorite
T. pedum Ichnospecies (Ciabeghodsi et al., 2007; Shahkarami et al., 2017b; Famarini Bozchaloui et al., 2020)
Sampling interval
Ediacaran-Cambrian boundary:
*1: Shahkarami et al. (2017a, b)
*2: Etemad-Saeed et al. (2021)
*3: Hamdi et al. (1989); Ciabeghodsi (2007)
*4: Famarini Bozchalouei et al. (2020)
B
Period
Formation
Member
Cambrian
Ediacaran
Soltanieh
Kahar
UDM
USM
MDM
LSM
LDM
*4
*3
*2
*1
1100 m
1000 m
900 m
800 m
700 m
600 m
500 m
400 m
300 m
200 m
100 m
0 m
P
Tubular macrofossils horizon

Figure 2

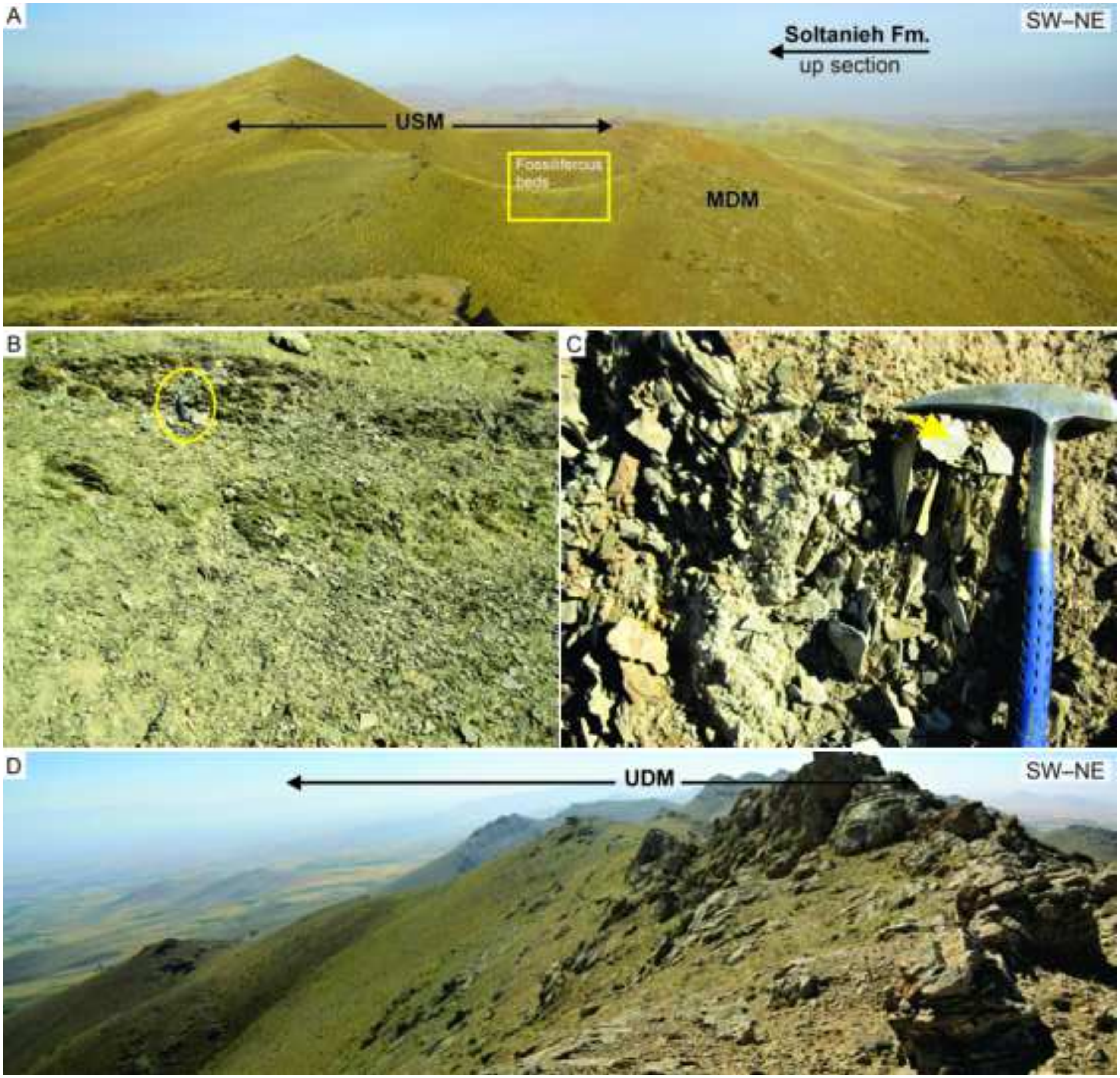
A
SW–NE
Soltanieh Fm.
up section
USM
Fossiliferous beds
MDM
B
C
D
UDM
SW–NE

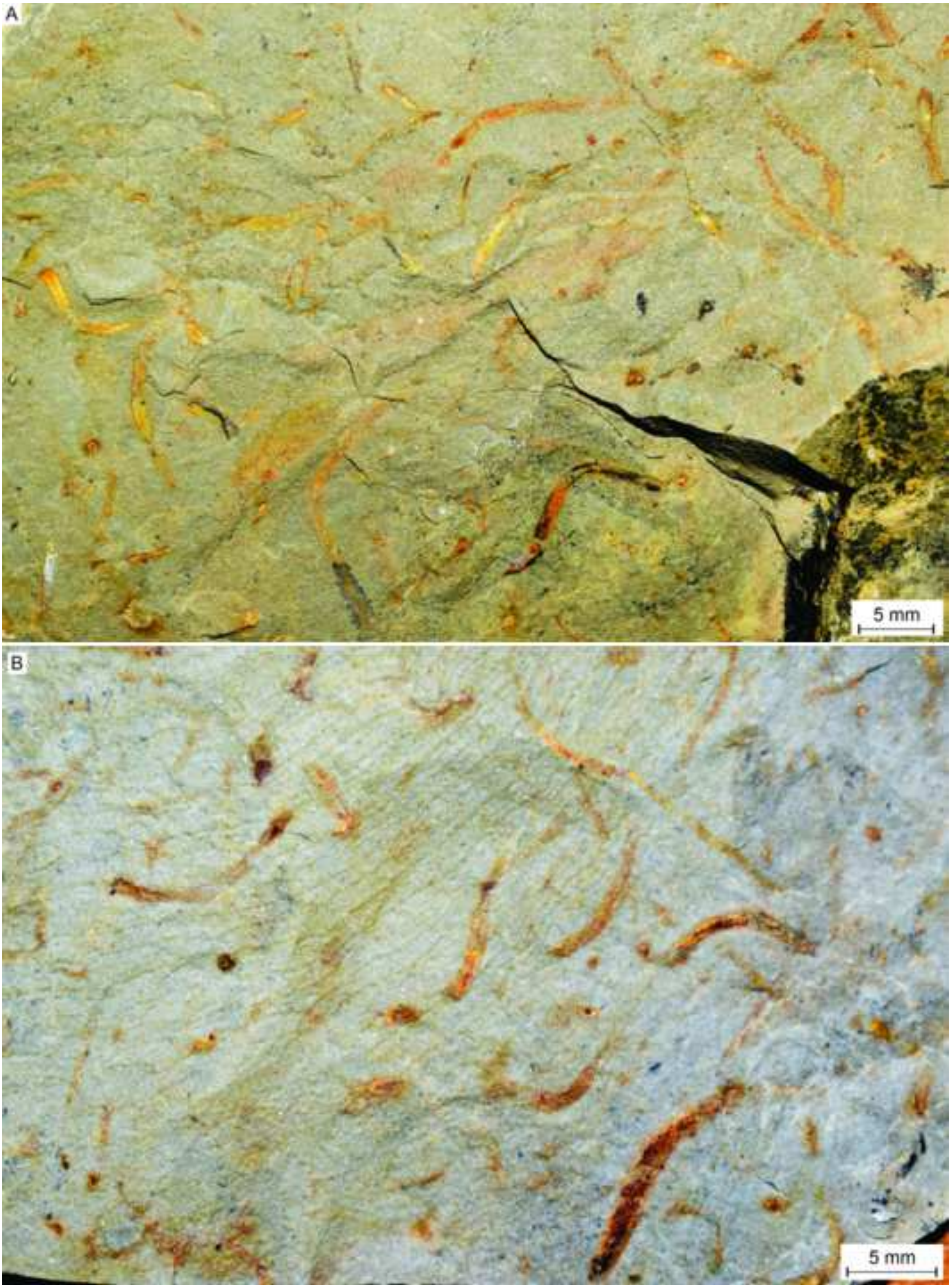
A
5 mm
B
5 mm

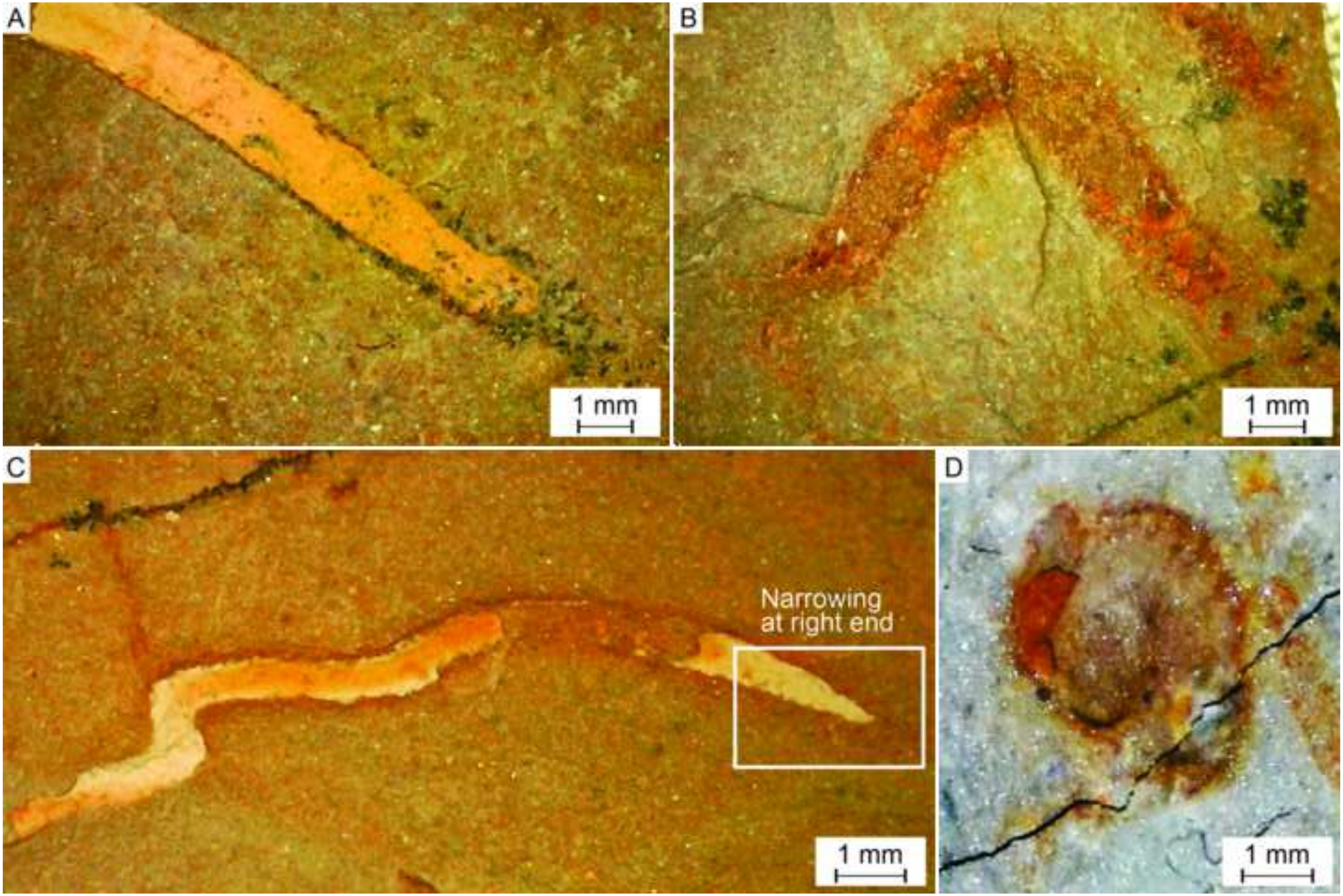
A
1 mm
B
1 mm
C
Narrowing at right end
1 mm
D
1 mm

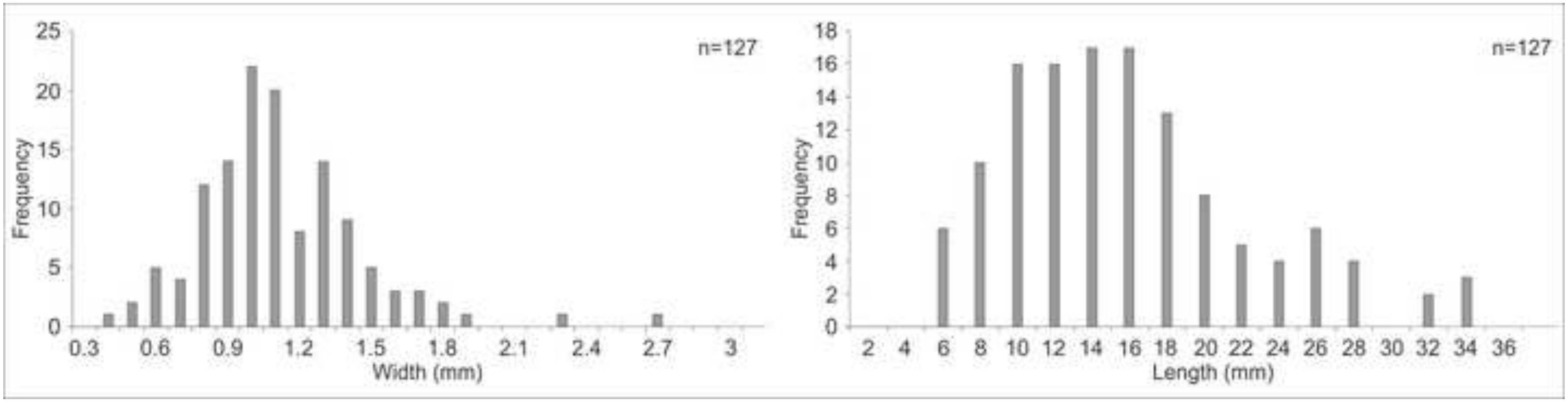

25
20
15
10
5
0
Frequency
n=127
0.3
0.6
0.9
1.2
1.5
1.8
2.1
2.4
2.7
3
Width (mm)
18
16
14
12
10
8
6
4
2
0
Frequency
n=127
2
4
6
8
10
12
14
16
18
20
22
24
26
28
30
32
34
36
Length (mm)

Figure 6

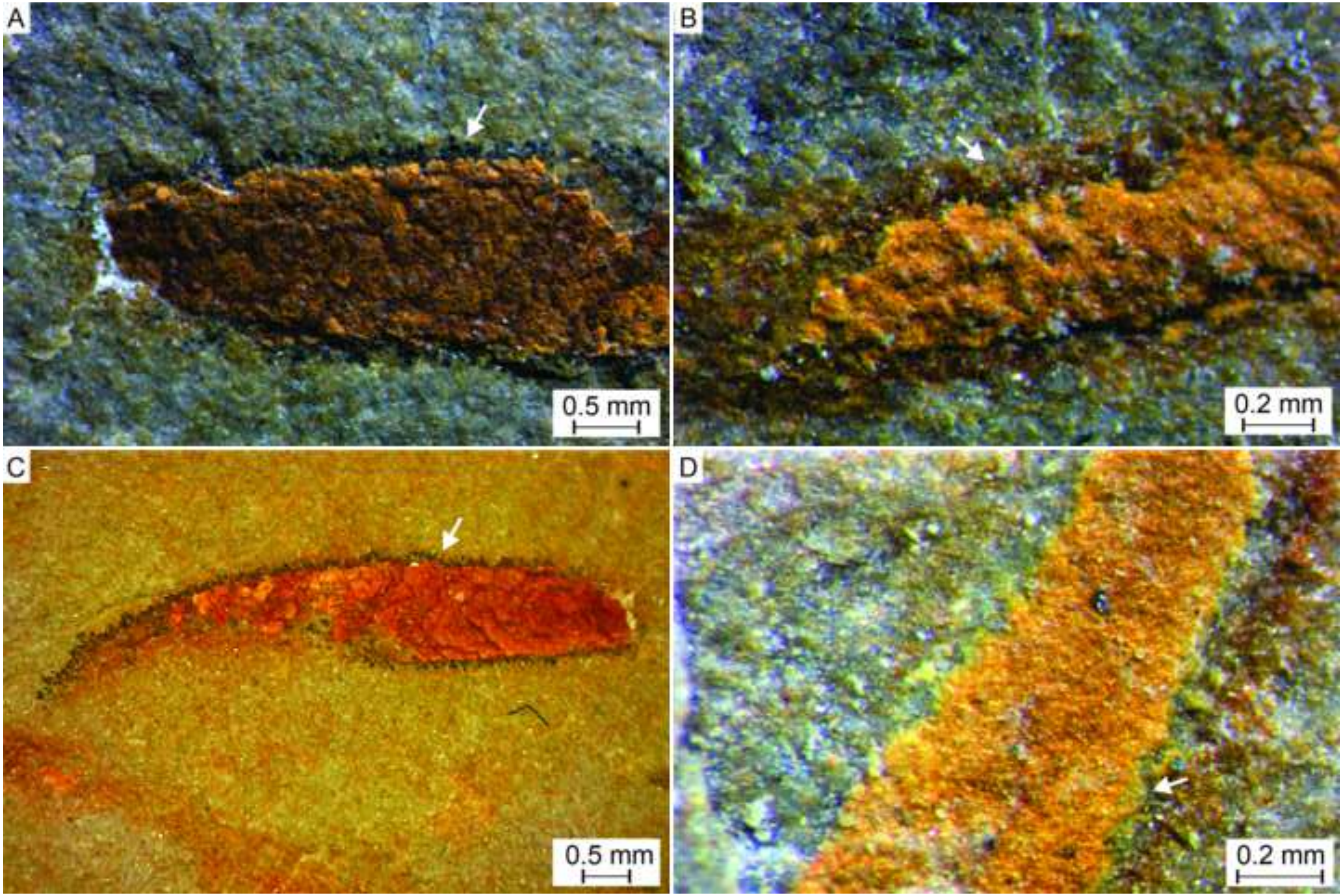

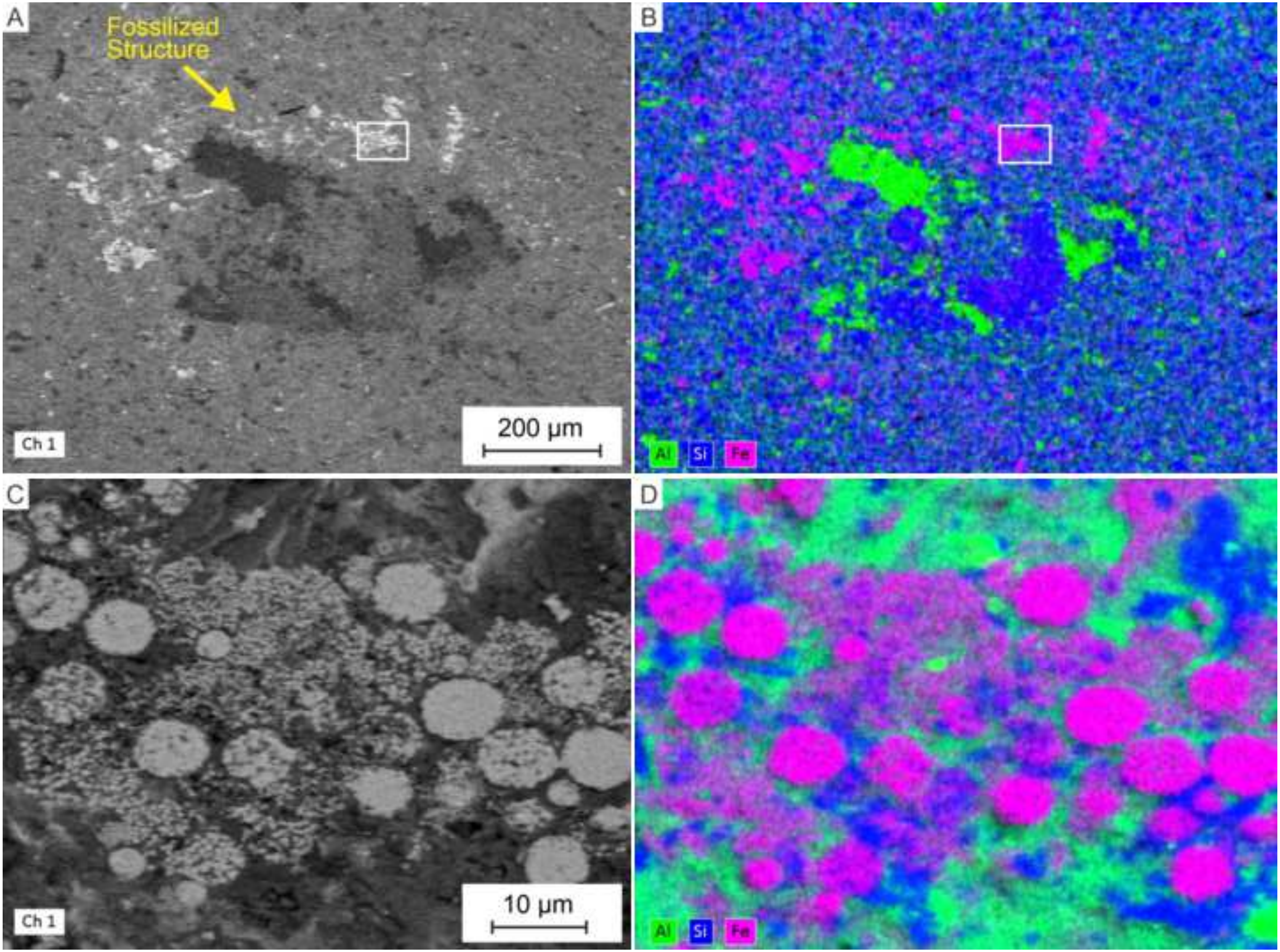
A
Fossilized Structure
Ch 1
200 μm
B
Al
Si
Fe
C
Ch 1
10 μm
D
Al
Si
Fe

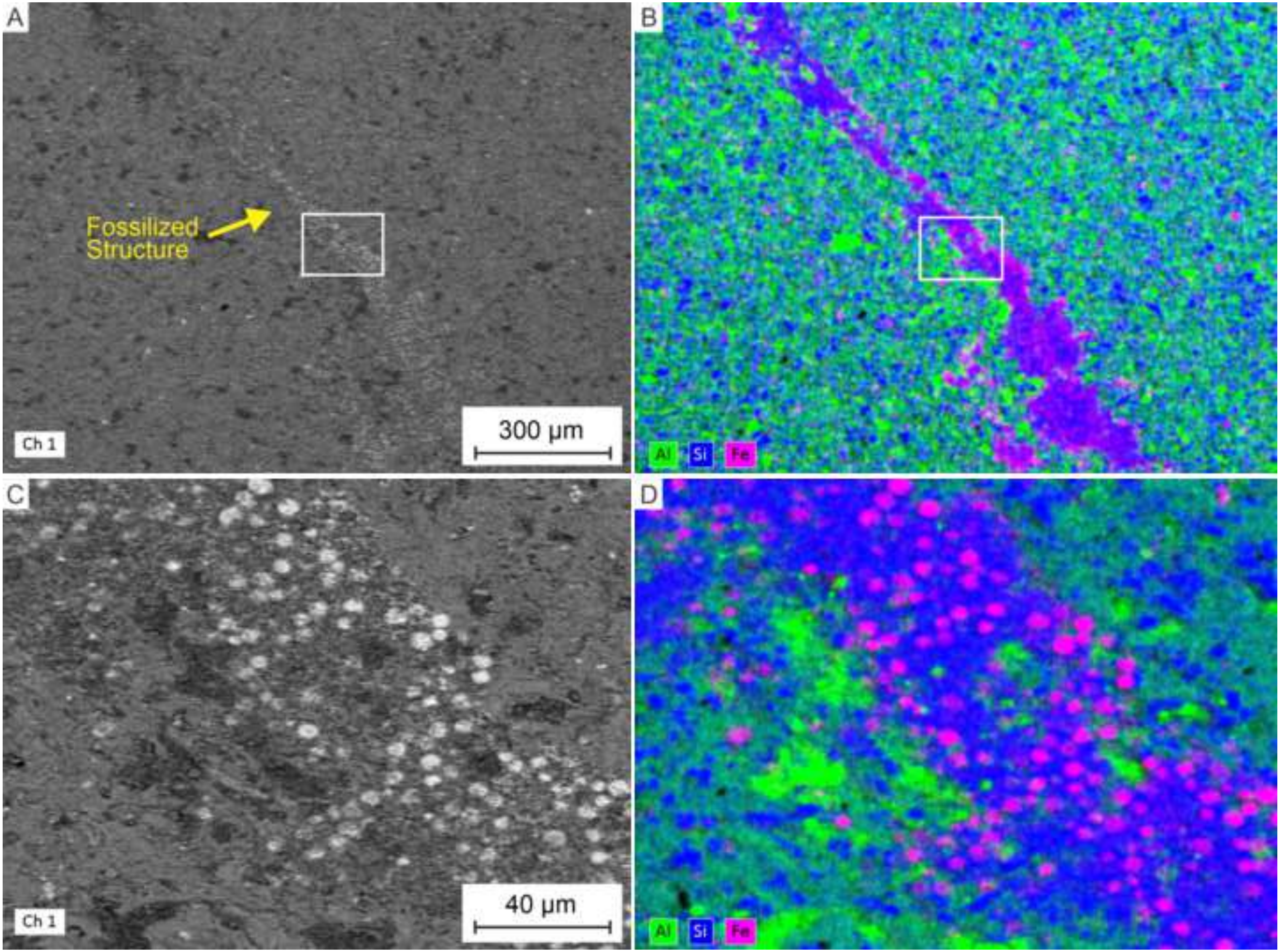
A
Fossilized Structure
Ch 1
300 µm
B
Al
Si
Fe
C
Ch 1
40 µm
D
Al
Si
Fe

Figure 9

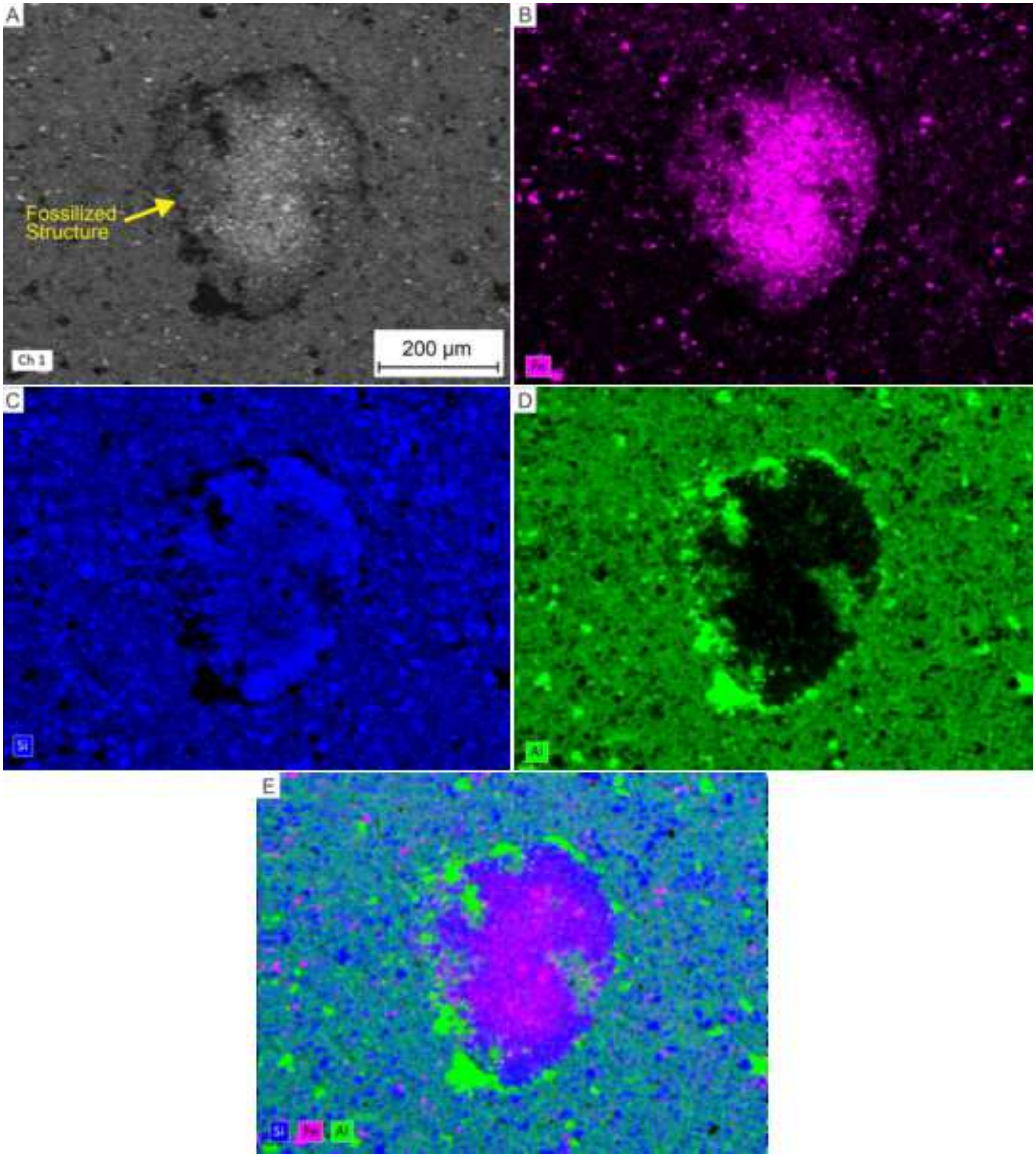

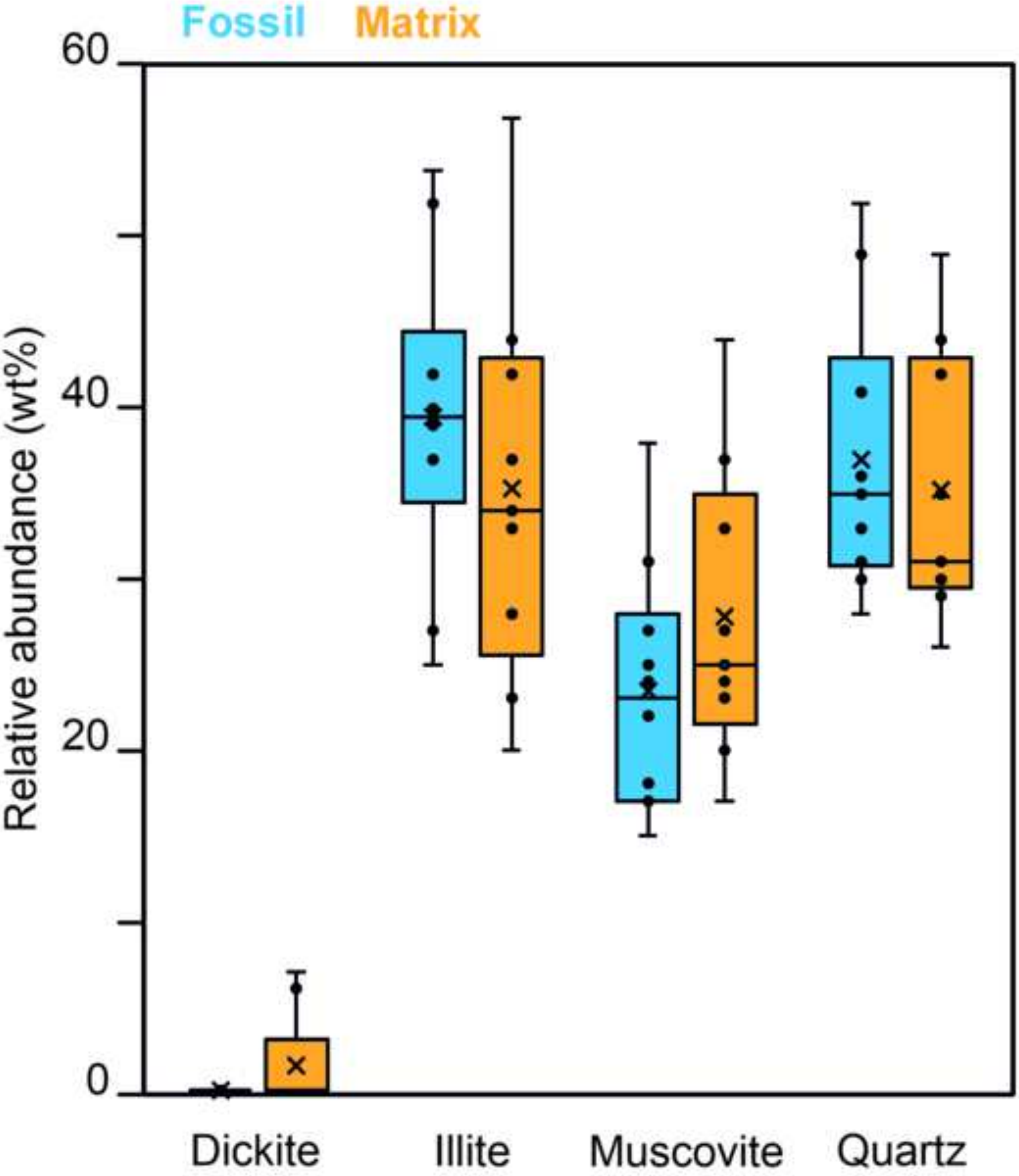
Fossil
Matrix
Relative abundance (wt%)
60
40
20
0
Dickite
Illite
Muscovite
Quartz